

O-TPT: Orthogonality Constraints for Calibrating Test-time Prompt Tuning in Vision-Language Models

Ashshak Sharifdeen^{1,2}, Muhammad Akhtar Munir¹, Sanoojan Baliah¹, Salman Khan^{1,3},
Muhammad Haris Khan¹

¹Mohamed bin Zayed University of AI, ²University of Colombo, ³Australian National University
{ashshak.sharifdeen, muhammad.haris}@mbzui.ac.ae

Abstract

Test-time prompt tuning for vision-language models (VLMs) is getting attention because of their ability to learn with unlabeled data without fine-tuning. Although test-time prompt tuning methods for VLMs can boost accuracy, the resulting models tend to demonstrate poor calibration, which casts doubts on the reliability and trustworthiness of these models. Notably, more attention needs to be devoted to calibrating the test-time prompt tuning in vision-language models. To this end, we propose a new approach, called O-TPT that introduces orthogonality constraints on the textual features corresponding to the learnable prompts for calibrating test-time prompt tuning in VLMs. Towards introducing orthogonality constraints, we make the following contributions. First, we uncover new insights behind the suboptimal calibration performance of existing methods relying on textual feature dispersion. Second, we show that imposing a simple orthogonalization of textual features is a more effective approach towards obtaining textual dispersion. We conduct extensive experiments on various datasets with different backbones and baselines. The results indicate that our method consistently outperforms the prior state of the art in significantly reducing the overall average calibration error. Also, our method surpasses the zero-shot calibration performance on fine-grained classification tasks. Our code is available at <https://github.com/ashshaksharifdeen/O-TPT>.

1. Introduction

In recent years, vision-language models (VLMs), for example, CLIP [35], have shown impressive zero-shot inference abilities in various downstream tasks [18, 35]. VLMs align web-scale image-text data to learn a shared embedding space, enabling it to classify instances from novel categories in a zero-shot manner via carefully designed prompt templates. So, constructing these manually designed prompts is crucial for effective zero-shot transfer. However, such man-

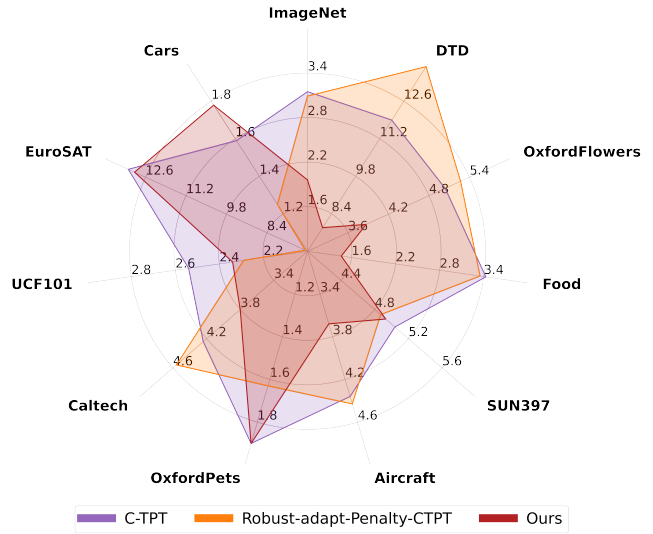


Figure 1. Comparison of calibration performance (ECE) with C-TPT [43] and Robust-adapt-Penalty-CTPT[29]. **Lower** the ECE better the calibration.

ually crafted prompts depend on domain-specific heuristics, which may limit their effectiveness [37]. Prompt tuning aims to learn prompts using downstream training data [46, 47]; however, learned prompts struggle to generalize beyond the task and training data. In addition, prompt-tuning methods require labeled data, which can be costly or even unavailable.

Recently, test-time prompt tuning [37] has emerged as a paradigm for refining prompts during inference, enabling VLMs to better adapt to newer tasks without labeled data and retraining. However, while prompt tuning at the test-time has been shown to enhance the accuracy of the VLM, it usually results in poorly calibrated predictions, which means that the confidence of the model does not align well with its accuracy [29, 43]. This lack of calibration raises concerns about the trustworthiness of VLMs in applications that demand reliable uncertainty estimates, such as health-

care [17, 40] or autonomous systems [4, 44, 48]. Poorly calibrated predictions can lead to overconfidence, which can lead to undesirable consequences in safety-critical applications, where decisions often depend on model outputs. We note that calibration in test-time prompt tuning for VLMs remains largely unexplored.

We note that calibration in test-time prompt tuning for VLMs remains largely unexplored with very few attempts. A recent method C-TPT [43] observes that test-time prompt tuning methods [37] often sacrifice the model’s calibration performance while boosting its accuracy, leading to unreliable prediction confidence for possibly many test examples. It shows that enhancing text feature dispersion can mitigate the overconfidence issue arising in test-time prompt tuning. However, the method could struggle to ensure the desired dispersion in challenging cases. This can lead to the underutilization of the textual feature space, potentially resulting in textual features lying in close proximity (Fig. 3) and eventually causing poor calibration performance (Fig. 1).

We note that the core methodology of C-TPT [43] overlooks the critical relationship between the angular separation among textual features and the calibration performance. Our findings reveal a strong correlation: textual features with lower cosine similarity (i.e., greater angular separation) between them lead to an improved calibration, as indicated by a lower Expected Calibration Error (ECE) (Fig. 2). Armed with this insight, we propose to impose orthogonalization constraints on the textual features by enforcing the angular distance between them. As such, this allows us to effectively utilize the feature space. Due to improved text feature separation, we observe superior calibration performance (Fig. 1). Our contributions are summarized as follows:

- We provide new insights underlying the suboptimal performance of an existing top-performing calibration method for the prompt testing-time tuning of VLMs.
- We propose a novel approach (named O-TPT) for calibrating test-time prompt tuning of VLMs by enforcing orthogonality constraints. This is accomplished by introducing orthogonal regularization on the textual features.
- We perform an extensive evaluation to validate our approach in various data sets and in different baselines. The results reveal that our O-TPT delivers consistent gains over the state-of-the-art methods in overall average calibration performance with several different baselines. Moreover, our O-TPT provides better calibration performance than the zero-shot CLIP, which reveals improved calibration compared to existing SOTA.

2. Related Work

Prompt tuning for vision-language models (VLMs): VLMs like CLIP [35] and ALIGN [18] leveraged large datasets of image-text pairs to create shared embedding

spaces that align images with their textual descriptions [25]. This cross-modal alignment enables impressive zero-shot performance across various domains by applying hand-crafted prompt templates. As a result, models can predict without additional training on new tasks. The embeddings are optimized through contrastive learning by matching image-text pairs in a latent space, which enhances the model’s ability to understand the relationship between visual and textual data. Since the design of handcrafted prompts requires domain-specific heuristics, they could be suboptimal for various newer domains. This led to the development of prompt-tuning methods that treat prompts as trainable embeddings. A notable example is CoOP [47], which refined prompts in CLIP [35] using labeled samples, leading to better classification performance. Building upon this, CoCoOP [46] addressed the limitations of CoOP [47] by enhancing generalization to out-of-distribution data, effectively improving the model’s ability to new, unseen domains. Recent advancements in prompt tuning, such as Test-Time Prompt Tuning (TPT) [37], have introduced algorithms to refine prompts on-the-fly using a single example during inference using entropy minimization. TPT has successfully enhanced model accuracy in zero-shot scenarios. However, it ends up worsening the calibration performance by making overconfident predictions.

Calibration of deep neural networks: Calibration evaluates how closely a model’s predicted confidence aligns with its accuracy. It is crucial for high-stakes applications that demand trustworthy uncertainty estimates, such as healthcare and autonomous systems [7]. Post hoc calibration techniques, such as Temperature Scaling (TS) [8], are employed to improve prediction reliability by scaling the model’s logits using a temperature variable. This temperature variable is learned on a hold-out validation set. However, such post-hoc methods often depend on the availability of labeled datasets that closely match the target data distribution [21]. Such datasets are rarely available in zero-shot and out-of-distribution contexts. To address this challenge, train-time calibration methods have been proposed, which typically employ auxiliary loss as regularizers with the task-specific loss during model training. Some notable examples of train-time calibration methods for object classification [11, 21, 32] and object detection [26–28] focused on reducing model overconfidence, leading to enhanced reliability in model predictions. However, these are supervised train-time calibration methods and are not directly applicable to scenarios where data is unlabeled, such as in the test-time prompt tuning of CLIP-like models.

Calibration & VLMs: VLMs show good performance in zero-shot settings due to their extensive training on large-scale image-text pairs. However, when adapting these models to new domains or tasks, they often demonstrate poor calibration *i.e.* the prediction confidence does not corre-

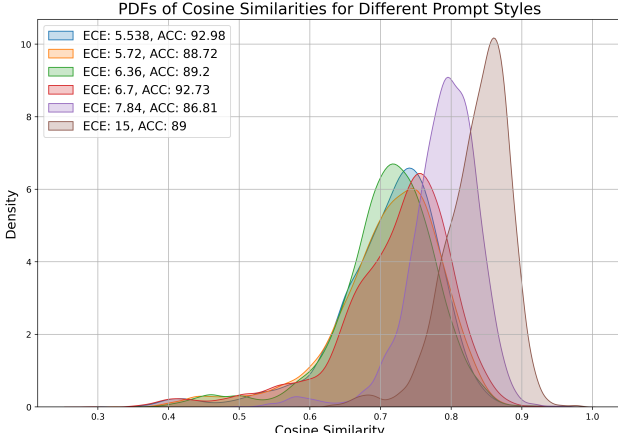


Figure 2. Probability Density Functions of intra-text feature cosine similarities

spond to the actual likelihood of correctness. Methods based on test time prompting such as TPT [37] can improve task-specific accuracy, but could increase model overconfidence by expanding the logit range. To address these calibration challenges, [29] introduced logit normalization techniques. Zero-shot logit normalization refines the logits in reference to (original) zero-shot settings, thereby maintaining the calibration of the model’s confidence levels. Continuing in similar lines, [29] proposed sample adaptive logit scaling, which normalizes logits per sample during inference. The work of [43] examined the dispersion of text features in VLMs and suggested that well-calibrated prompts tend to produce text embeddings with a broader dispersion between different classes [43]. By maximizing this dispersion, the calibration error can be reduced without compromising accuracy. To capture this characteristic, they proposed Average Text Feature Dispersion (ATFD) loss as a quantitative measure.

However, we observe that this approach could be limited in establishing enough dispersion in challenging cases. This primarily happens due to underutilization of the space, and so the textual features can lie quite close to each other. We develop a new approach that introduces orthogonalization constraints on textual features by enforcing the angular distance between them. This allows us to effectively disperse textual features, and hence better utilize the space, leading to consistently better calibration performance.

3. Methodology

3.1. Preliminaries

CLIP-based Zero-shot Classification: CLIP [35] is a vision-language model that learns a joint embedding space for images and texts by contrastive training on a vast dataset of image-text pairs. It consists of two encoders: a text encoder \mathbf{f}_T and an image encoder \mathbf{f}_I , which map text and im-

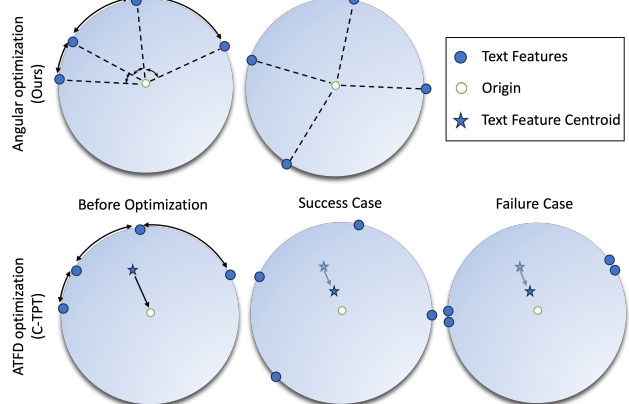


Figure 3. Comparison of angular optimization (ours) and ATFD optimization (C-TPT) [43]

age inputs into a shared space. In the zero-shot classification setting, CLIP classifies images by leveraging language prompts to represent each class. For each class c_i in the set of classes $C = \{c_1, c_2, c_3, \dots, c_N\}$, we construct a textual prompt \mathbf{t}_{c_i} using a hand-crafted template such as “*a photo of a {class}*”, where “{class}” is class name. Each text prompt \mathbf{t}_{c_i} is fed into the text encoder to obtain a text feature vector: $\mathbf{e}_{c_i} = \mathbf{f}_T(\mathbf{t}_{c_i})$, for $i = 1, 2, \dots, N$. This results in a set of text embeddings $\{\mathbf{e}_{c_1}, \mathbf{e}_{c_2}, \dots, \mathbf{e}_{c_N}\}$ that represent the classes in the shared embedding space. A test image I is processed through the image encoder to produce an image embedding: $\mathbf{v} = \mathbf{f}_I(I)$. To determine how well the image matches each class, we compute the cosine similarity between the image embedding \mathbf{v} and each text embedding \mathbf{e}_{c_i} : $s_i = \cos(\mathbf{v}, \mathbf{e}_{c_i})$. Higher scores indicate greater similarity and alignment in the embedding space. The similarity scores are converted into probabilities using the Softmax function with a temperature parameter τ . The temperature τ controls the smoothness of the Softmax distribution; a smaller τ sharpens it, increasing confidence in top predictions by amplifying score differences. The predicted class \hat{c} for the image I is the one with the highest probability: $\hat{c} = \arg \max_{c_i} P(c_i|I)$. The corresponding predicted confidence is: $\hat{P} = \max_{c_i} P(c_i|I)$. This enables an efficient classification across a wide range of categories without the need for additional fine-tuning.

Transitioning from hand-crafted prompts, prompt tuning has been applied in CLIP [2, 35, 42, 45, 46] to optimize text prompts using labeled ImageNet samples, achieving robust cross-dataset generalization. Alternatively, TPT [37] fine-tunes prompts at inference without labeled data, though it may amplify calibration error due to overconfidence [9].

Defining and Measuring Calibration Error: Calibration is crucial for a model because it ensures that its predicted probabilities correspond accurately to the actual likelihood of the outcomes. We can define this as: $\mathbb{P}(\hat{c} = c | \hat{P} = p) =$

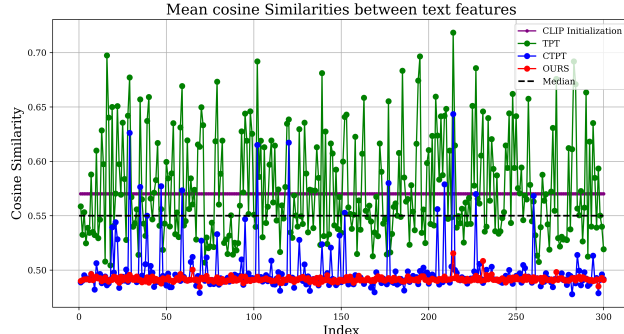


Figure 4. Mean cosine similarity changes comparison on a fine-grained dataset [30] with CLIP B/16 backbone. Our orthogonal constraint offers consistent cosine similarity values among text features for all the data points.

p . Here, the input image I and its corresponding ground truth label c have an associated predicted confidence $p = \hat{P}$, and the predicted class is \hat{c} . Calibration can be evaluated using the Expected Calibration Error (ECE) [33], which is computed as:

$$\text{ECE} = \sum_{m=1}^M \frac{|A_m|}{N} |\text{acc}(A_m) - \text{conf}(A_m)|, \quad (1)$$

where M defines the number of bins used to divide the predictions, A_m is the sample set with predicted confidence scores falling into the m -th bin. $|A_m|$ represents the number of samples in bin. N is the total number of predictions. $\text{acc}(A_m)$ is the accuracy of the predictions and $\text{conf}(A_m)$ is the average predicted confidence for the samples in bin A_m .

3.2. Orthogonal Constraint for Prompt Calibration

Why orthogonality? Different prompts can yield text features with similar classification accuracy, but their calibration performance can differ significantly. It has been demonstrated, well-calibrated text features are often more dispersed concerning L2 distance, which is spread farther apart in embedding space [43]. This analysis overlooked an important factor: angular relationships among text features, which can significantly affect calibration. We hypothesize that considering angular relationships among text features is important for understanding calibration of VLMs. Unlike existing methods (e.g., [43]) that rely solely on L2 distance for feature separation, our approach highlights significance of orthogonality among textual features.

To address this gap, we investigate the relationship between the cosine similarity of text features generated from various hand-crafted prompt styles. Our findings reveal a strong correlation: lower angular similarity between features corresponds to improved calibration. By encouraging greater angular separation (orthogonality), we ensure each feature points in a unique direction, sharpening class boundaries, and enhancing calibration robustness. As illustrated

Method	Metric	Group 1	Group 2	Overall
TPT	Acc	62.80	79.09	69.10
	ECE	15.97	9.45	13.45
CTPT	Acc	63.66	79.51	69.79
	ECE	6.04	4.27	5.06
O-TPT (Ours)	Acc	62.87	79.62	70.07
	ECE	4.75	3.80	3.87

Table 1. Comparison of Accuracy and Expected Calibration Error (ECE) across methods and categories based on the TPT[37] text features cosine similarity.

in Fig. 2, the probability density functions (PDFs) of cosine similarities across text feature pairs show that prompts yielding lower ECE are skewed toward lower cosine similarities. This suggests that promoting greater angular distinctiveness among text features can more effectively improve VLM calibration.

Comparison between dispersion and orthogonality: The ATFD loss in C-TPT [43] aims to disperse text features by moving their text features farther apart from their centroid. Still, it mainly affects the centroid’s position without ensuring adequate spacing between the individual features. In zero-shot CLIP inference, normalized text features reside on the surface of the unit hypersphere[36]. In ATFD, this could potentially drive the centroid of the text features toward the origin of the hypersphere by merely adjusting the features on the surface. However, this method may not effectively optimize the separation of features across the hypersphere’s surface. Towards achieving optimal calibration, we hypothesize that mere feature dispersion is insufficient and it is more effective to accomplish distinct angular separation between the features. To further validate our findings, we conducted an experiment on a fine-grained dataset [30]. For each data sample, we extract test-time prompt-tuned text features generated by TPT, C-TPT and our method (\circ -TPT), compute pairwise cosine similarities, and plot their mean, as shown in Fig. 4. The results show that TPT, which lacks calibration-specific constraints, exhibits high fluctuations in cosine similarity, reflecting its inconsistent calibration performance.

In Table 1, we present the accuracy and ECE results for each method, dividing data into two groups based on cosine similarities of TPT text features relative to median cosine similarity. Group 1 includes points with cosine similarity values above median, while Group 2 includes those below the median. We then calculate the ECE and accuracy separately for each group, allowing a more fine-grained analysis of each method’s performance. As hypothesized, points

with higher cosine similarity tend to show elevated ECE, indicating poor calibration and suggesting these are more challenging points. In these challenging cases (Group 1), our method significantly outperforms TPT as well as C-TPT in terms of calibration performance, resulting in an overall lower ECE. Interestingly, C-TPT, which applies dispersion in the L2 space, also struggles to calibrate, showing higher cosine similarities in cases where TPT fails (these challenging points), as illustrated in Fig. 3. In contrast, our method’s orthogonalization constraint consistently produces text features with much lower and more consistent cosine similarities compared to CLIP initialization, resulting in better calibration overall. Our orthogonalization method enforces angular distance between feature pairs, fully utilizing the hyperspherical space (Fig. 3). As such, promoting orthogonality enhances feature separation, leading to distinct class boundaries and improved calibration.

Orthogonalization constraint: Motivated by the aforementioned analyses, we introduce an orthogonalization-based approach that systematically enhances calibration by focusing on the angular properties of the text feature matrix. For each class c_i , we have a text feature vector $\mathbf{e}_{c_i} \in \mathbb{R}^D$. Let \mathbf{E} be the text feature matrix containing text features of all classes, $\mathbf{E} \in \mathbb{R}^{C \times D}$. E_{ij} represents the embedding value for i -th class in j -th dimension, where $i \in \{1, \dots, C\}$ indexes the classes and $j \in \{1, \dots, D\}$ represents the embedding dimensions. This matrix encapsulates the spatial distribution of text features between different classes. To enhance angular distances, we consider the matrix product $\mathbf{E}\mathbf{E}^T$, which contains pairwise cosine similarities, a direct measure of the angular distance, between the text features. Ideally, we want $\mathbf{E}\mathbf{E}^T$ to approximate the identity matrix I_C , indicating that all text features are orthogonal. To this end, we formulate a robust method by incorporating an orthogonalization constraint into the prompt tuning process, enhancing calibration performance of the test-time prompt tuning. The objective formulation is defined as:

$$\mathbf{t}^* = \arg \min_{\mathbf{t}} (L_{TPT} + \lambda \|\mathbf{E}\mathbf{E}^T - I_C\|_2^2) \quad (2)$$

where L_{TPT} is the TPT loss, λ is a hyperparameter balancing the two terms. This adjustment promotes a stable and uniformly distributed set of features across the hypersphere, directly addressing the ATFD loss’s angular spacing limitations and ensuring effective utilization of the full feature space. By explicitly enforcing orthogonality, we systematically enhance the angular separation between text features, leading to improved calibration.

4. Experiments

4.1. Experimental Setup

Datasets: We conduct our experiments using the ImageNet [5] and Caltech101 [6] datasets as well as different fine-

grained classification datasets across various domains. For texture classification, we use DTD [3]. The FLW [30] dataset comprises of flower categories. For food classification, we use Food101 [1]. SUN37 [41] dataset offers scene categorization, and the UCF[38] dataset is used for human action recognition. Vehicle classification datasets include StanfordCars [23] and Aircraft [24], while OxfordPets [34] covers pet animal categories. Additionally, EuroSAT [12] contains satellite imagery for environmental categorization. To evaluate out-of-distribution (OOD) performance, we use the ImageNet-A [13], ImageNet-V2, ImageNet-R [14], and ImageNet-S[39] datasets.

Implementation details: We utilize the CLIP-RN50 and CLIP ViT-B/16 architectures. In all experimental settings, we leverage TPT [37] as our baseline. To optimize the prompt, we use a single-step update with the AdamW optimizer [22], with a learning rate of 0.005. We also perform a linear algebra technique, HouseHolder transform [19] on top of $\mathbf{E}\mathbf{E}^T$ matrix to further enhance optimization at one test-time step. We use a batch size of 64 across all experiments. All experiments were performed on an NVIDIA RTX A6000 with 48GB of memory. We initialize the prompt embeddings as hard prompts, following the settings in C-TPT [43]. The remaining settings follow the configuration in [37]. We fix the λ as 18 across all experiments unless otherwise specified.

4.2. Results

We evaluate the calibration performance of our method (\textcircled{o} -TPT) applied to TPT with CLIP-B/16 and CLIP-RN50 backbones (Tables 2 & 3). \textcircled{o} -TPT which applies orthogonal constraints on text features significantly improves Expected Calibration Error (ECE) compared to both C-TPT [43] and Robust Adapt [29] (in combination with C-TPT). Using the CLIP-B/16 backbone, our method achieves an average ECE of **4.21**, outperforming C-TPT at 5.13 and Robust Adapt’s best result of 4.66. When applied to the CLIP-RN50 backbone, our approach reduces ECE to **5.45**, a substantial improvement over the 6.19 ECE achieved by C-TPT. Notably, our method also surpasses the zero-shot calibration performance showing lower ECE on both backbones, which is a feat unmatched by any other approach, while maintaining the high accuracy levels of TPT.

Results on natural distribution shifts: Table 4 presents results on natural distribution shift datasets, where all experimental configurations remain the same as those detailed in the implementation, with the exception of λ , which is set to 2 for these datasets. Across the ImageNet variant datasets, our \textcircled{o} -TPT method consistently achieves notable reductions in ECE on both the CLIP-RN50 and CLIP-ViT-B/16 backbones. On the CLIP-ViT-B/16 backbone, \textcircled{o} -TPT achieves an average ECE of **4.88**, a substantial improvement over C-TPT and TPT, which average 5.82 and 12.0, re-

Method	Metric	Inet	DTD	FLW	Food	SUN	Air	Pets	Calt	UCF	SAT	Car	Avg
Zero Shot	Acc.	66.7	44.3	67.3	83.6	62.5	23.9	88.0	92.9	65.0	41.3	65.3	63.7
	ECE	2.12	8.50	3.00	2.39	2.53	5.11	4.37	5.50	3.59	13.89	4.25	4.43
TPT	Acc.	69.0	46.7	69.0	84.7	64.5	23.4	87.1	93.8	67.3	42.4	66.3	65.0
	ECE	10.6	21.2	13.5	3.98	11.3	16.8	5.77	4.51	2.54	13.2	5.16	11.6
C-TPT	Acc	68.5	46	69.8	83.7	64.8	24.85	88.2	93.63	65.7	43.2	65.8	64.57
	ECE	3.15	11.9	5.04	3.43	5.04	4.36	1.9	4.24	2.54	13.2	1.59	5.13
Robust-adapt-SaLs-CTPT	Acc.	68.04	45.51	69.43	83.18	64.38	23.94	88.12	93.63	65.32	43.05	65.48	64.55
	ECE	2.63	14.56	2.74	1.26	3.56	6.21	3.16	3.78	6.96	14.92	2.82	5.69
Robust-adapt-Penalty-CTPT	Acc.	68.04	45.69	69.55	83.28	64.36	23.91	87.95	93.47	65.32	44.06	65.53	64.65
	ECE	2.63	13.9	5.27	3.35	4.87	4.43	1.63	4.56	2.29	7.08	1.25	4.66
Robust-adapt-ZS-CTPT	Acc	68.01	45.63	69.55	83.25	64.41	23.88	88.03	93.31	65.24	42.64	65.45	64.51
	ECE	3.01	12.35	4.94	3.8	5.16	4.31	2.06	4.34	2.17	12.23	1.7	5.09
O-TPT (Ours)	Acc.	67.33	45.68	70.07	84.13	64.23	23.64	87.95	93.95	64.16	42.84	64.53	64.41
	ECE	1.96	7.88	3.87	1.46	4.93	3.68	1.9	3.8	2.34	12.98	1.78	4.23

Table 2. Comparison of calibration performance with CLIP-ViT-B/16 backbone. The overall best-performing result is in bold.

Method	Metric	Inet	DTD	FLW	Food	SUN	Air	Pets	Calt	UCF	SAT	Car	Avg
Zero Shot	Acc.	58.1	40.0	61.0	74.0	58.6	15.6	83.8	85.8	58.4	23.7	55.7	55.9
	ECE	2.09	9.91	3.19	3.11	3.54	6.45	5.91	4.33	3.05	15.4	4.70	5.61
TPT	Acc.	60.7	41.5	62.5	74.9	61.1	17.0	84.5	87.0	59.5	28.3	58.0	57.7
	ECE	11.4	25.7	13.4	5.25	9.24	16.1	3.65	5.04	12.4	22.5	3.76	11.7
C-TPT	Acc.	60.2	42.2	65.2	74.7	61.0	17.0	84.1	86.9	59.7	27.8	56.5	57.75
	ECE	3.01	19.8	4.14	1.86	2.93	10.7	2.77	2.07	3.83	15.1	1.94	6.19
Robust-adapt-SaLs-CTPT	Acc.	60.02	41.37	65.0	74.71	60.46	16.83	83.73	86.53	59.56	27.54	56.27	57.20
	ECE	2.21	9.2	2.29	1.45	3.32	5.6	3.6	4.38	4.2	10.46	2.53	6.82
Robust-adapt-Penalty-CTPT	Acc.	60.06	41.55	64.88	74.69	60.47	17.01	83.84	86.45	59.42	26.64	56.4	57.40
	ECE	5.93	21.18	4.03	1.83	2.81	10.85	3.3	2.7	3.93	11.97	1.99	6.41
Robust-adapt-ZS-CTPT	Acc.	60.0	41.72	64.92	74.07	60.37	16.71	83.61	86.65	59.6	27.64	56.26	57.41
	ECE	2.85	15.01	3.39	3.44	8.24	7.21	6.11	4.66	4.13	9.91	4.85	6.34
O-TPT (Ours)	Acc.	58.97	41.9	65.61	74.22	60.85	16.77	83.4	86.86	58.84	28.35	56.44	57.47
	ECE	3.1	16.53	2.5	1.2	3.2	8.18	3.5	2.75	2.6	14.71	1.69	5.45

Table 3. Comparison of calibration performance with CLIP-RN50 backbone. The overall best-performing result is in bold.

spectively. Similarly, on the CLIP-RN50 backbone, O-TPT achieves an average ECE of **9.69**, outperforming C-TPT and TPT, which reach ECE values of 12.1 and 16.7, respectively. These results highlight the effectiveness of our approach in handling natural distribution shifts.

4.3. Ablation Studies

Comparison with post-hoc method: Fig. 5 illustrates the impact of ECE across fine-grained datasets using calibration techniques applied to TPT [37]. We compare TPT,

C-TPT [43], TPT with temperature scaling [9] (a classical post-processing technique adjusting pre-softmax logits with a temperature value trained on a separate validation set), and our proposed method, O-TPT. As shown in Fig. 5, O-TPT consistently achieves superior calibration, demonstrating its effectiveness in enhancing model reliability across datasets.

Addressing Under and Over-Confidence: As shown in Tables 2 and 3, our proposed method outperforms most fine-grained datasets on both ResNet-50 and ViT-B/16 back-

Method	Metric	I-A	I-V2	I-R	I-S	Avg
CLIP-ViT-B/16	Acc.	47.8	60.8	74.0	46.1	57.2
	ECE	8.61	3.01	3.58	4.95	5.04
TPT	Acc.	52.6	63.0	76.7	47.5	59.9
	ECE	16.4	11.1	4.36	16.1	12.0
C-TPT	Acc.	51.6	62.7	76.0	47.9	59.6
	ECE	8.16	6.23	1.54	7.35	5.82
O-TPT (Ours)	Acc.	49.87	61.65	72.55	47.12	57.80
	ECE	7.22	3.97	1.46	6.87	4.88
CLIP-RN50	Acc.	21.7	51.4	56.0	33.3	40.6
	ECE	21.3	3.33	2.07	3.15	7.46
TPT	Acc.	25.2	54.6	58.9	35.1	43.5
	ECE	31.0	13.1	9.18	13.7	16.7
C-TPT	Acc.	23.4	54.7	58.0	35.1	42.8
	ECE	25.4	8.58	4.57	9.70	12.1
O-TPT (Ours)	Acc.	23.07	53.11	54.47	33.98	41.16
	ECE	24.56	3.87	4.47	5.85	9.69

Table 4. Calibration performance comparison with TPT (baseline) using CLIP-B/16 (top) and CLIP- RN50 (bottom) backbones in natural distribution shifts datasets.

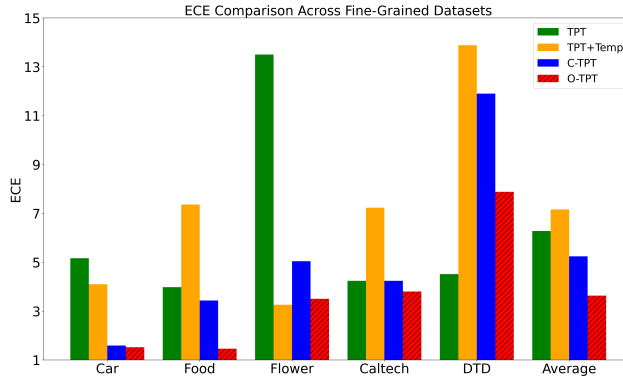


Figure 5. Calibration performance comparison with post-hoc method across fine-grained datasets.

bones. However, these tables do not indicate whether our approach addresses overconfidence or underconfidence. Fig.6 displays reliability diagrams for ViT-B/16 on the Food, Flower, and DTD datasets. In Fig.6a, C-TPT [43] shows underconfidence for the Food dataset, which is rectified with our O-TPT calibration method, as shown in Fig.6d. Additionally, our method better addresses overconfidence issues, as illustrated in Fig.6e and 6f, when compared to Fig.6b and 6c, respectively.

Standard deviation across different seeds run: Table 5 shows the mean and standard deviation for accuracy and ECE across five datasets, each with three different seed runs. Our method reports a lower mean standard deviation in accuracy, providing more stable performance regardless of the randomness in the prompt initialization. Additionally, our method has a lower mean standard deviation in ECE

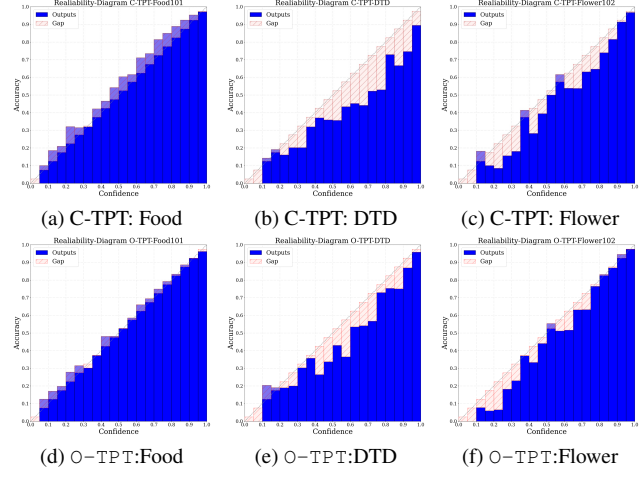


Figure 6. Reliability diagrams.

compared to C-TPT, indicating greater consistency in calibration. This robustness in both accuracy and calibration makes our approach particularly valuable for applications where stable performance across multiple runs is essential.

Other Baselines: Beyond tuning prompt parameters at inference time, we applied supervised-trained prompt embedding parameters to evaluate their calibration effectiveness with our O-TPT method during test-time prompt tuning. Specifically, we used the officially published checkpoints of CoOp [47] and MAPLE [20]. For MAPLE, we employed the Base-to-Novel checkpoints. As shown in Table 6, for CoOp across 10 fine-grained datasets, our method demonstrates significant improvement on 8 datasets, reducing the overall average ECE to **7.91**. This represents a substantial improvement over C-TPT + CoOp and TPT + CoOp, which yield overall ECE values of 10.4 and 18.36, respectively. Similarly, when evaluating our method O-TPT with MAPLE under test-time prompt tuning, we observe notable calibration improvements across most datasets compared to using TPT + MAPLE alone. In Table 7, our approach achieves an overall ECE reduction to **4.11**, compared to 6.94 for TPT + MAPLE. Overall, integrating O-TPT with supervised-trained prompt embedding parameters during test-time prompt tuning maintains accuracy and significantly improves calibration performance.

Impact of HouseHolder transformation: Table 8 presents the impact of applying Householder transformation. This transformation further improves our performance.

SCE performance comparison: In addition to ECE, we report calibration performance with Static Calibration Error (SCE) [31], a class-wise extension of ECE. Table 9 compares the calibration performance of our method against other approaches. Across the three datasets, O-TPT consistently outperforms the alternatives, achieving an average SCE reduction of up to **0.65**, which marks a substantial im-

Method	Metric	DTD	FLW	Food	Caltech	Car	Avg
C-TPT	Std. Acc	0.12	0.16	0.16	0.22	0.2	0.17
	Std. ECE	0.24	0.18	0.24	0.12	0.19	0.194
O-TPT (Ours)	Std. Acc	0.14	0.11	0.03	0.10	0.19	0.11
	Std. ECE	0.17	0.25	0.14	0.20	0.10	0.177

Table 5. Standard deviation across three different seed runs.

Method	Metric	DTD	FLW	Food	SUN	Air	Pets	Calt	UCF	SAT	Car	Avg
TPT+CoOp	Acc.	44.5	68.7	83.8	65.6	20.0	89.1	94.0	67.2	40.6	65.6	63.91
	ECE	34.8	19.9	9.66	20.8	29.6	7.40	3.65	19.9	31.3	6.63	18.36
TPT+CoOp+C-TPT	Acc.	45.0	69.0	83.7	65.1	19.2	89.3	93.9	66.6	40.7	63.1	63.56
	ECE	21.0	10.2	4.49	11.8	21.5	2.12	1.66	12.0	13.2	2.45	10.04
TPT+CoOp+O-TPT	Acc.	45.45	68.57	83.55	64.01	18.69	89.07	93.71	65.64	40.17	64.12	63.14
	ECE	16.02	6.81	3.59	7.23	16.82	1.92	0.92	9.16	13.76	2.85	7.91

Table 6. Calibration performance when using CoOP as a baseline and CLIP-ViT-B/16 backbone.

Method	Metric	DTD	FLW	Food	SUN	Air	Pets	Calt	UCF	SAT	Car	Avg
TPT+MAPLE	Acc.	50.05	70.72	85.01	64.87	24.36	87.78	94.42	66.48	47.32	66.5	65.75
	ECE	11.8	11.63	1.78	8.47	10.58	1.79	2.38	7.41	9.42	4.14	6.94
TPT+MAPLE+O-TPT	Acc.	49.11	71.53	84.35	63.49	24	89.97	92.29	65.82	44.58	65.38	65.05
	ECE	4.9	4.35	1.49	2.78	6.41	3.97	3.49	2.22	7.92	3.61	4.11

Table 7. Calibration performance when using Maple as a baseline and CLIP-ViT-B/16 backbone.

Method	Metric	INet	DTD	FLW	Food	SUN	Air	Pets	Calt	UCF	SAT	Car	Avg
O-TPT without HouseHolder	Acc.	67.32	45.69	69.18	84.25	64.11	23.82	88.03	93.35	65.16	42.83	65.00	64.34
	ECE	1.96	8.61	3.94	1.66	5.28	3.59	1.93	4.21	2.19	13.89	1.71	4.45
O-TPT (Ours)	Acc.	67.33	45.68	70.07	84.13	64.23	23.64	87.95	93.95	64.16	42.84	64.53	64.41
	ECE	1.96	7.88	3.87	1.46	4.93	3.68	1.9	3.8	2.34	12.98	1.78	4.23

Table 8. Calibration performance of our O-TPT with and without HouseHolder transformation.

Method	DTD	FLW	Calt	Avg
Zero-shot	1.34	0.59	0.25	0.73
TPT	1.42	0.50	0.16	0.69
C-TPT	1.31	0.52	0.22	0.68
O-TPT	1.24	0.53	0.17	0.65

Table 9. Static Calibration Error (SCE) (10^{-2}) performance comparison with CLIP-ViT-B/16 backbone.

provement over Zero-shot, TPT, and C-TPT, with average SCE values of 0.73, 0.69, and 0.68, respectively. See supplementary for SCE results on additional datasets.

5. Conclusion

We propose a new approach to calibrate test-time prompt tuning in vision-language models. Our preliminary analyses reveal that the higher angular distances between textual features while prompt learning are correlated to lower calibration error. We note that, achieving orthogonality between textual features is more effective than obtaining dispersion through L2 distance-based objectives. Therefore, we propose orthogonal regularization on textual features during test-time prompt tuning which is named as O-TPT. Our method consistently records state-of-the-art performance with different backbones and baselines.

References

- [1] Lukas Bossard, Matthieu Guillaumin, and Luc Van Gool. Food-101 – mining discriminative components with random forests. In *European Conference on Computer Vision*, 2014. 5
- [2] Guangyi Chen, Weiran Yao, Xiangchen Song, Xinyue Li, Yongming Rao, and Kun Zhang. Plot: Prompt learning with optimal transport for vision-language models, 2023. 3
- [3] Mircea Cimpoi, Subhransu Maji, Iasonas Kokkinos, Sammy Mohamed, and Andrea Vedaldi. Describing textures in the wild. In *Proceedings of the IEEE conference on computer vision and pattern recognition*, pages 3606–3613, 2014. 5
- [4] Can Cui, Yunsheng Ma, Xu Cao, Wenqian Ye, Yang Zhou, Kaizhao Liang, Jintai Chen, Juanwu Lu, Zichong Yang, Kuei-Da Liao, et al. A survey on multimodal large language models for autonomous driving. In *Proceedings of the IEEE/CVF Winter Conference on Applications of Computer Vision*, pages 958–979, 2024. 2
- [5] Jia Deng, Wei Dong, Richard Socher, Li-Jia Li, Kai Li, and Li Fei-Fei. Imagenet: A large-scale hierarchical image database. In *2009 IEEE conference on computer vision and pattern recognition*, pages 248–255. Ieee, 2009. 5
- [6] Li Fei-Fei, Rob Fergus, and Pietro Perona. Learning generative visual models from few training examples: An incremental bayesian approach tested on 101 object categories. *Computer Vision and Pattern Recognition Workshop*, 2004. 5
- [7] Zoubin Ghahramani. Probabilistic machine learning and artificial intelligence. *Nature*, 521(7553):452–459, 2015. 2
- [8] Chuan Guo, Geoff Pleiss, Yu Sun, and Kilian Q Weinberger. On calibration of modern neural networks. In *International conference on machine learning*, pages 1321–1330. PMLR, 2017. 2
- [9] Chuan Guo, Geoff Pleiss, Yu Sun, and Kilian Q. Weinberger. On calibration of modern neural networks. In *Proceedings of the 34th International Conference on Machine Learning*, pages 1321–1330. PMLR, 2017. 3, 6
- [10] Asif Hanif, Fahad Shamshad, Muhammad Awais, Muzammal Naseer, Fahad Shahbaz Khan, Karthik Nandakumar, Salman Khan, and Rao Muhammad Anwer. Baple: Backdoor attacks on medical foundational models using prompt learning, 2024. 4
- [11] Ramya Hebbalaguppe, Jatin Prakash, Neelabh Madan, and Chetan Arora. A stitch in time saves nine: A train-time regularizing loss for improved neural network calibration. In *Proceedings of the IEEE/CVF Conference on Computer Vision and Pattern Recognition*, pages 16081–16090, 2022. 2
- [12] Patrick Helber, Benjamin Bischke, Andreas Dengel, and Damian Borth. Introducing eurosat: A novel dataset and deep learning benchmark for land use and land cover classification. In *IGARSS 2018-2018 IEEE International Geoscience and Remote Sensing Symposium*, pages 204–207. IEEE, 2018. 5
- [13] Dan Hendrycks, Kevin Zhao, Steven Basart, Jacob Steinhardt, and Dawn Song. Natural adversarial examples. *arXiv preprint arXiv:1907.07174*, 2019. 5
- [14] Dan Hendrycks, Steven Basart, Norman Mu, Saurav Kadavath, Frank Wang, Evan Dorundo, Rahul Desai, Tyler Zhu, Samyak Parajuli, Mike Guo, Dawn Song, Jacob Steinhardt, and Justin Gilmer. The many faces of robustness: A critical analysis of out-of-distribution generalization. *arXiv preprint arXiv:2006.16241*, 2020. 5
- [15] Yijin Huang, Pujin Cheng, Roger Tam, and Xiaoying Tang. Fine-grained prompt tuning: A parameter and memory efficient transfer learning method for high-resolution medical image classification, 2024. 4
- [16] Noor Hussein, Fahad Shamshad, Muzammal Naseer, and Karthik Nandakumar. Promptssmooth: Certifying robustness of medical vision-language models via prompt learning, 2024. 4
- [17] Zhanghexuan Ji, Mohammad Abuzar Shaikh, Dana Moukheiber, Sargur N Srihari, Yifan Peng, and Mingchen Gao. Improving joint learning of chest x-ray and radiology report by word region alignment. In *Machine Learning in Medical Imaging: 12th International Workshop, MLMI 2021, Held in Conjunction with MICCAI 2021, Strasbourg, France, September 27, 2021, Proceedings 12*, pages 110–119. Springer, 2021. 2
- [18] Chao Jia, Yinfei Yang, Ye Xia, Yi-Ting Chen, Zarana Parekh, Hieu Pham, Quoc Le, Yun-Hsuan Sung, Zhen Li, and Tom Duerig. Scaling up visual and vision-language representation learning with noisy text supervision. In *International conference on machine learning*, pages 4904–4916. PMLR, 2021. 1, 2
- [19] Linda Kaufman. The generalized householder transformation and sparse matrices. *Linear Algebra and its Applications*, 90:221–234, 1987. 5
- [20] Muhammad Uzair Khattak, Hanoona Rasheed, Muhammad Maaz, Salman Khan, and Fahad Shahbaz Khan. Maple: Multi-modal prompt learning, 2023. 7
- [21] Bingyuan Liu, Ismail Ben Ayed, Adrian Galdran, and Jose Dolz. The devil is in the margin: Margin-based label smoothing for network calibration. In *Proceedings of the IEEE/CVF Conference on Computer Vision and Pattern Recognition*, pages 80–88, 2022. 2
- [22] Ilya Loshchilov and Frank Hutter. Decoupled weight decay regularization, 2019. 5
- [23] S. Maji, J. Kannala, E. Rahtu, M. Blaschko, and A. Vedaldi. Fine-grained visual classification of aircraft. Technical report, 2013. 5
- [24] Subhransu Maji, Esa Rahtu, Juho Kannala, Matthew Blaschko, and Andrea Vedaldi. Fine-grained visual classification of aircraft. *arXiv preprint arXiv:1306.5151*, 2013. 5
- [25] Sachit Menon and Carl Vondrick. Visual classification via description from large language models. In *The Eleventh International Conference on Learning Representations*, 2023. 2
- [26] Muhammad Akhtar Munir, Muhammad Haris Khan, M Sarfraz, and Mohsen Ali. Towards improving calibration in object detection under domain shift. *Advances in Neural Information Processing Systems*, 35:38706–38718, 2022. 2

- [27] Muhammad Akhtar Munir, Muhammad Haris Khan, Salman Khan, and Fahad Shahbaz Khan. Bridging precision and confidence: A train-time loss for calibrating object detection. In *Proceedings of the IEEE/CVF Conference on Computer Vision and Pattern Recognition*, pages 11474–11483, 2023.
- [28] Muhammad Akhtar Munir, Salman H Khan, Muhammad Haris Khan, Mohsen Ali, and Fahad Shahbaz Khan. Cal-detr: calibrated detection transformer. *Advances in neural information processing systems*, 36, 2024. 2
- [29] Balamurali Murugesan, Julio Silva-Rodríguez, Ismail Ben Ayed, and Jose Dolz. Robust calibration of large vision-language adapters. *ECCV*, 2024. 1, 3, 5
- [30] Maria-Elena Nilsback and Andrew Zisserman. Automated flower classification over a large number of classes. In *2008 Sixth Indian conference on computer vision, graphics & image processing*, pages 722–729. IEEE, 2008. 4, 5
- [31] Jeremy Nixon, Michael W. Dusenberry, Linchuan Zhang, Ghassen Jerfel, and Dustin Tran. Measuring calibration in deep learning. In *Proceedings of the IEEE/CVF Conference on Computer Vision and Pattern Recognition (CVPR) Workshops*, 2019. 7
- [32] Jongyoun Noh, Hyekang Park, Junghyup Lee, and Bumsub Ham. Rankmixup: Ranking-based mixup training for network calibration. In *Proceedings of the IEEE/CVF International Conference on Computer Vision*, pages 1358–1368, 2023. 2
- [33] Mahdi Pakdaman Naeini, Gregory Cooper, and Milos Hauskrecht. Obtaining well calibrated probabilities using bayesian binning. *Proceedings of the AAAI Conference on Artificial Intelligence*, 29(1), 2015. 4
- [34] Omkar M Parkhi, Andrea Vedaldi, Andrew Zisserman, and CV Jawahar. Cats and dogs. In *2012 IEEE conference on computer vision and pattern recognition*, pages 3498–3505. IEEE, 2012. 5
- [35] Alec Radford, Jong Wook Kim, Chris Hallacy, Aditya Ramesh, Gabriel Goh, Sandhini Agarwal, Girish Sastry, Amanda Askell, Pamela Mishkin, Jack Clark, et al. Learning transferable visual models from natural language supervision. In *International conference on machine learning*, pages 8748–8763. PMLR, 2021. 1, 2, 3
- [36] Peiyang Shi, Michael C Welle, Mårten Björkman, and Danica Kragic. Towards understanding the modality gap in clip. In *ICLR 2023 workshop on multimodal representation learning: perks and pitfalls*, 2023. 4
- [37] Manli Shu, Weili Nie, De-An Huang, Zhiding Yu, Tom Goldstein, Anima Anandkumar, and Chaowei Xiao. Test-time prompt tuning for zero-shot generalization in vision-language models. *Advances in Neural Information Processing Systems*, 35:14274–14289, 2022. 1, 2, 3, 4, 5, 6
- [38] Khurram Soomro, Amir Roshan Zamir, and Mubarak Shah. Ucf101: A dataset of 101 human actions classes from videos in the wild. *arXiv preprint arXiv:1212.0402*, 2012. 5
- [39] Haohan Wang, Songwei Ge, Zachary Lipton, and Eric P Xing. Learning robust global representations by penalizing local predictive power. In *Advances in Neural Information Processing Systems*, pages 10506–10518, 2019. 5
- [40] Zifeng Wang, Zhenbang Wu, Dinesh Agarwal, and Jimeng Sun. Medclip: Contrastive learning from unpaired medical images and text. In *Proceedings of the 2022 Conference on Empirical Methods in Natural Language Processing*, pages 3876–3887, 2022. 2
- [41] Jianxiong Xiao, Krista A Ehinger, James Hays, Antonio Torralba, and Aude Oliva. Sun database: Exploring a large collection of scene categories. *International Journal of Computer Vision*, 119:3–22, 2016. 5
- [42] Hantao Yao, Rui Zhang, and Changsheng Xu. Visual-language prompt tuning with knowledge-guided context optimization. In *Proceedings of the IEEE/CVF Conference on Computer Vision and Pattern Recognition (CVPR)*, pages 6757–6767, 2023. 3
- [43] Hee Suk Yoon, Eunseop Yoon, Joshua Tian Jin Tee, Mark Hasegawa-Johnson, Yingzhen Li, and Chang D Yoo. C-ptt: Calibrated test-time prompt tuning for vision-language models via text feature dispersion. *International conference on machine learning*, 2024. 1, 2, 3, 4, 5, 6, 7
- [44] Junwei You, Haotian Shi, Zhuoyu Jiang, Zilin Huang, Rui Gan, Keshu Wu, Xi Cheng, Xiaopeng Li, and Bin Ran. V2x-vlm: End-to-end v2x cooperative autonomous driving through large vision-language models. *arXiv preprint arXiv:2408.09251*, 2024. 2
- [45] Kaiyang Zhou, Jingkang Yang, Chen Change Loy, and Ziwei Liu. Learning to prompt for vision-language models. *International Journal of Computer Vision*, 130(9):2337–2348, 2022. 3
- [46] Kaiyang Zhou, Jingkang Yang, Chen Change Loy, and Ziwei Liu. Conditional prompt learning for vision-language models. In *Proceedings of the IEEE/CVF conference on computer vision and pattern recognition*, pages 16816–16825, 2022. 1, 2, 3
- [47] Kaiyang Zhou, Jingkang Yang, Chen Change Loy, and Ziwei Liu. Learning to prompt for vision-language models. *International Journal of Computer Vision*, 130(9):2337–2348, 2022. 1, 2, 7
- [48] Xingcheng Zhou, Mingyu Liu, Ekim Yurtsever, Bare Luka Zagar, Walter Zimmer, Hu Cao, and Alois C Knoll. Vision language models in autonomous driving: A survey and outlook. *IEEE Transactions on Intelligent Vehicles*, 2024. 2

O-TPT: Orthogonality Constraints for Calibrating Test-time Prompt Tuning in Vision-Language Models

Supplementary Material

In this supplementary material, we provide the following:

1. We reveal the relation between calibration performance and angular distances (sec. A1)
2. We compare the SCE performance (sec. A2)
3. Reliability plots comparison with C-TPT [43]. (sec. A3)
4. Calibration performance with different hard prompt styles (sec. A4)
5. Calibration with a Combination of C-TPT and O-TPT (sec. A5)
6. O-TPT results on Medical Prompt tuning methods (sec. A6)
7. Pareto Front analysis with varying λ (sec. A7)

A1. Relation Between Calibration Performance and Angular Distances

To further validate our motivation, we conduct an experiment using 80 different hard prompt styles [35] to evaluate their corresponding Expected Calibration Error (ECE) performance and the mean cosine similarity of text features. This evaluation is performed on zero-shot inference using the CLIP-B/16 backbone. Figure 7 illustrates the results for prompts that yield higher accuracies across seven diverse datasets: Flower, Caltech101, SUN397, Cars, Pets, UCF101, and Food101. Specifically, we focus on the top 10 prompt styles that provide the highest accuracies.

The results reveal a clear trend between mean cosine similarity (an angular distance measure) and ECE (calibration performance). A lower mean cosine similarity correlates with a reduced ECE, indicating that greater angular distancing among text features promotes better calibration. This suggests that prompts with text features exhibiting greater angular distances between their representations lead to improved calibration outcomes.

A2. SCE performance comparison

Tables 10 and 11 present the Static Calibration Error (SCE) results across 10 datasets using CLIP-B/16 and CLIP RN-50 backbones. Our method, O-TPT, outperforms C-TPT on both backbones, achieving an overall average SCE values of **1.07** for CLIP-B/16 and **1.24** for CLIP RN-50, demonstrating improved calibration performance.

A3. Reliability Plots

Figure 8 and Figure 9 illustrate the reliability diagrams for the CLIP-B/16 and CLIP RN-50 backbones, respectively,

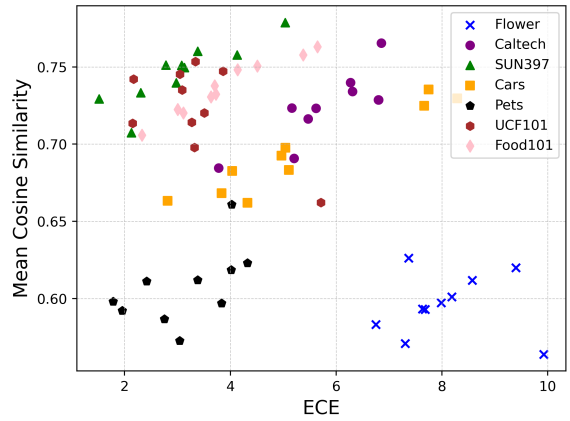


Figure 7. Relation of ECE with cosine similarities (of textual features) on CLIP-B/16 backbone.

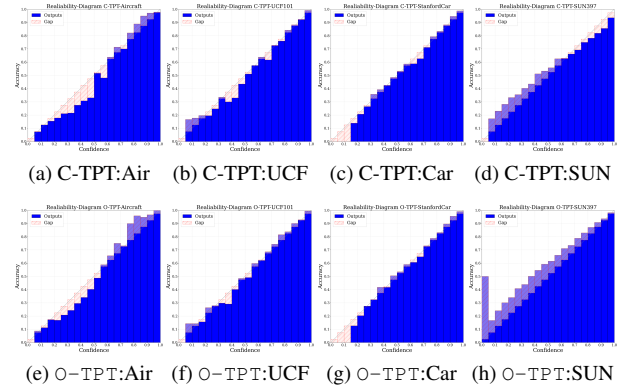


Figure 8. Reliability diagrams for CLIP-B/16.

comparing the performance of C-TPT and O-TPT across the Aircraft, UCF101, Car, and SUN397 datasets. For the CLIP-B/16 backbone (Fig. 8), O-TPT effectively addresses the overconfidence problem and outperforms C-TPT, as evident from the reliability diagrams in the top and bottom rows of Fig. 8. Similarly, with CLIP RN-50 backbone, (Fig. 9) shows that O-TPT provides significantly better calibration compared to C-TPT, particularly in addressing overconfident predictions.

A4. Calibration with different prompts

This section presents the results of O-TPT initialized with different prompts, such as ‘a photo of the cool {class}’

Method	Metric	DTD	FLW	Food	SUN	Air	Pets	CalT	UCF	SAT	Car	Avg
Zero Shot	SCE	1.33	0.59	0.20	0.12	0.52	0.68	0.25	0.52	6.18	0.23	1.06
TPT	SCE	1.44	0.51	0.17	0.15	0.58	0.60	0.16	0.57	7.07	0.25	1.15
C-TPT	SCE	1.31	0.52	0.22	0.14	0.56	0.58	0.22	0.52	6.81	0.22	1.11
O-TPT (Ours)	SCE	1.24	0.53	0.19	0.12	0.56	0.57	0.17	0.51	6.58	1.07	1.07

Table 10. Static Calibration Error (SCE) (10^{-2}) performance comparison with CLIP-B/16 backbone.

Method	Metric	DTD	FLW	Food	SUN	Air	Pets	CalT	UCF	SAT	Car	Avg
Zero Shot	SCE	1.31	0.66	0.29	0.12	0.54	0.73	0.35	0.54	7.39	0.23	1.22
TPT	SCE	1.52	0.63	0.25	0.11	0.60	0.54	0.38	0.51	8.23	0.24	1.30
C-TPT	SCE	1.43	0.62	0.26	0.11	0.53	0.67	0.32	0.51	8.07	0.23	1.27
O-TPT (Ours)	SCE	1.34	0.60	0.27	0.12	0.51	0.69	0.3	0.5	7.85	0.22	1.24

Table 11. Static Calibration Error (SCE) (10^{-2}) performance comparison with CLIP-RN-50 backbone.

Method	Metric	DTD	FLW	Food	SUN	Air	Pets	CalT	UCF	SAT	Car	Avg
Zero Shot	Acc.	38.4	64.5	81.4	62.4	22.7	86.2	88.1	67.6	34.6	66.5	61.24
	ECE	7.43	4.59	1.10	6.11	2.83	7.43	14.1	2.65	14.1	4.59	7.01
TPT	Acc.	45.5	67.9	84.9	65.9	24.5	87.4	91.5	66.4	43.3	67.2	64.45
	ECE	20.0	14.6	5.74	13.3	19.2	6.34	3.11	14.1	18.2	6.36	12.09
C-TPT	Acc.	46.3	69.6	84.1	65.5	24.7	88.8	91.7	67.0	43.0	66.9	64.76
	ECE	18.0	10.6	2.43	10.7	10.5	1.59	1.89	7.42	8.73	1.64	7.35
O-TPT (Ours)	Acc.	44.62	68.29	84.82	63.05	23.16	88.28	91.48	64.74	44.81	66.02	63.92
	ECE	12.85	4.67	1.85	2.67	6.37	3.59	3.0	4.08	8.33	2.71	5.01

Table 12. Comparison of calibration performance with CLIP-B/16 backbone with the prompt of ‘a photo of the cool {class}’

Method	Metric	DTD	FLW	Food	SUN	Air	Pets	CalT	UCF	SAT	Car	Avg
Zero Shot	Acc.	39.6	57.7	73.0	56.5	16.1	79.8	80.9	56.3	21.9	56.9	60.24
	ECE	6.94	5.14	1.49	3.33	6.42	3.30	4.79	3.76	13.9	4.83	5.39
TPT	Acc.	39.2	61.6	75.8	60.2	17.4	82.6	86.5	59.7	26.3	58.8	56.81
	ECE	24.8	17.0	7.93	11.4	17.5	7.31	6.02	14.4	15.7	4.49	12.65
C-TPT	Acc.	39.1	67.0	76.0	60.3	17.4	83.5	87.1	59.6	26.1	57.2	57.33
	ECE	18.0	6.34	3.70	8.28	13.5	1.75	2.85	8.82	11.2	1.65	7.61
O-TPT (Ours)	Acc.	40.54	65.49	75.51	58.98	15.99	83.78	86.98	58.79	26.89	56.77	56.97
	ECE	12.42	3.03	1.32	3.35	8.36	4.47	3.53	3.27	7.21	2.74	4.97

Table 13. Comparison of calibration performance with CLIP-RN-50 backbone with the prompt of ‘a photo of the cool {class}’

and ‘an example of {class}’, across CLIP-B/16 and CLIP RN-50 backbones. Tables 12 and 13 summarize the performance of O-TPT with the prompt ‘a photo of the cool

{class}’ and 5 context token tuning. For CLIP-B/16, O-TPT achieves an overall reduced calibration error of **5.01**, compared to 7.35 for C-TPT, while for RN-50, it

Method	Metric	DTD	FLW	Fod	SUN	Air	Pets	Cal	UCF	SAT	Car	Avg
Zero Shot	Acc.	42.4	64.7	83.9	61.4	22.3	82.5	90.9	64.8	38.8	64.6	61.63
	ECE	4.94	4.70	2.78	3.33	7.09	2.91	7.51	2.79	13.4	2.49	5.64
TPT	Acc.	45.8	69.4	84.8	65.3	22.9	83.0	93.0	67.1	40.7	67.3	63.93
	ECE	20.5	12.2	5.05	7.94	16.2	7.30	2.91	11.6	20.8	6.26	11.07
C-TPT	Acc.	45.4	71.5	84.3	66.0	23.6	86.9	93.8	66.4	51.5	66.6	65.6
	ECE	15.5	4.49	1.36	3.54	9.05	2.89	1.62	3.87	5.18	1.75	4.93
O-TPT (Ours)	Acc.	45.45	70.32	84.79	64.5	22.77	87.76	93.35	65.4	51.011	66.25	65.16
	ECE	11.79	3.22	2.92	4.62	7.92	3.29	3.24	2.63	5.08	1.92	4.66

Table 14. Comparison of calibration performance with CLIP-B/16 backbone with the prompt of ‘an example of {class}’

Method	Metric	DTD	FLW	Fod	SUN	Air	Pets	Cal	UCF	SAT	Car	Avg
Zero Shot	Acc.	41.10	58.10	75.20	56.20	16.10	75.70	80.30	56.30	25.5	55.8	48.45
	ECE	5.20	3.04	3.31	3.68	4.80	2.52	7.91	3.76	9.43	4.80	4.845
TPT	Acc.	41.2	62.7	76.1	60.7	17.9	77.2	87.1	57.7	29.4	57.7	56.77
	ECE	20.2	12.2	4.83	8.19	15.2	6.98	5.12	15.3	11.1	5.52	10.46
C-TPT	Acc.	41.2	65.4	75.8	61.4	17.6	78.0	88.4	58.4	30.4	57.1	57.37
	ECE	15.6	2.97	1.90	4.84	7.16	2.72	2.89	6.99	7.69	2.05	5.48
O-TPT (Ours)	Acc.	41.19	65.49	75.62	60.97	16.71	77.79	88.36	57.94	33.32	56.733	57.412
	ECE	13.59	2.49	1.47	3.38	6.6	2.55	2.56	6.2	5.07	2.69	4.66

Table 15. Comparison of calibration performance with CLIP- RN-50 backbone with the prompt of ‘an example of {class}’

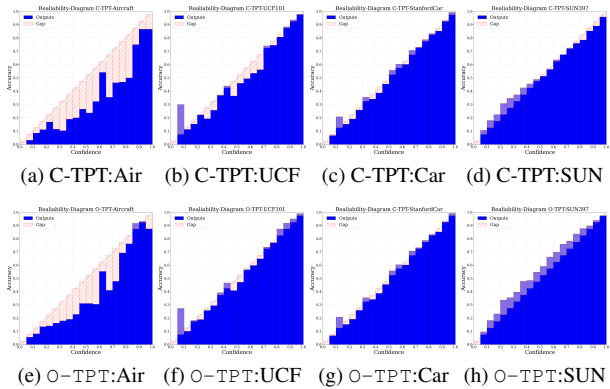


Figure 9. Reliability diagrams for CLIP RN-50.

achieves **4.97**, compared to 7.61 for C-TPT. Similarly, Tables 14 and 15 present the results for the prompt ‘an example of {class}’ and 4 context token tuning. Here, O-TPT again outperforms C-TPT, achieving a reduced calibration error of **4.66** (CLIP-B/16) compared to 4.93, and **4.66** (CLIP RN-50) compared to 5.48. These results consistently demonstrate that O-TPT effectively reduces calibration errors across various prompt initializations, showcasing its robustness and adaptability in diverse settings.

robustness and adaptability in diverse settings.

A5. Calibration with a Combination of C-TPT and O-TPT

Tab. 16 shows that O-TPT + C-TPT can outcompete O-TPT in calibration performance, thereby revealing the generalizability of O-TPT over a stronger baseline.

Method	Metric	DTD	FLW	UCF
O-TPT	ACC	45.68	70.07	64.16
	ECE	7.88	3.87	2.34
O-TPT + C-TPT	ACC	45.2	70.6	64.1
	ECE	7.06	3.41	2.14

Table 16. O-TPT + C-TPT on DTD,FLW and UCF.

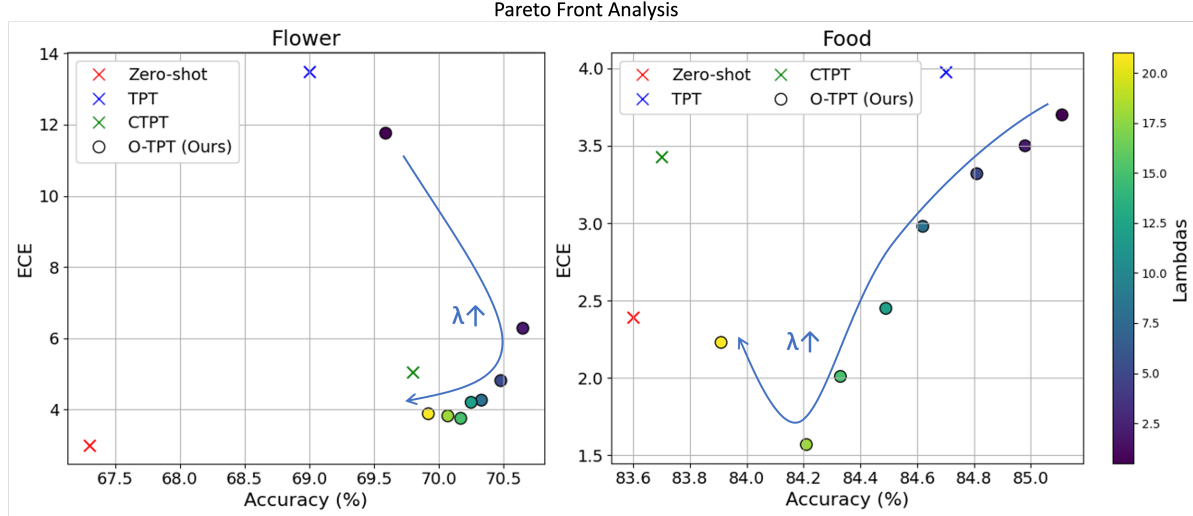


Figure 10. Pareto front analysis

Method	Metric	Covid(BA)	Covid(CA)
BAPLe	ACC	99.90	82.5
	ECE	3.21	15.64
BAPLe+ O-TPT	ACC	99.62	81.36
	ECE	0.91	5.97

Table 17. MedCLIP: BAPLe + O-TPT on Covid dataset.

Method	Metric	ISIC'18
FPT	ACC	98.43
	ECE	0.2328
FPT+ O-TPT	ACC	98.25
	ECE	0.1381

Table 18. FPT+O-TPT on ISIC2018.

Method	Metric	KC
PS	ACC	76.6
	ECE	15.54
PS+ O-TPT	ACC	76.2
	ECE	12.73

Table 19. PLIP: Promptssmooth (PS)+O-TPT on KatherColon (KC).

A6. O-TPT results on Medical Prompt tuning methods

In Tab.18, we evaluate FPT[15] and FPT+O-TPT on ISIC2018, showing encouraging ECE reduction while maintaining accuracy. Tab.19 provides comparison using PLIP with Prompt Smooth (PS)[16], where PS+O-TPT improves calibration. Similarly, Tab.17 provides comparison using MedCLIP with BAPLe[10] where BAPLe+O-TPT improves calibration.

A7. Pareto Front analysis with varying lamdas

Fig. 10 shows the Pareto front analysis on Food and Flower datasets, highlighting the accuracy-ECE tradeoff with varying λ s. Our method achieves a better balance than TPT and C-TPT across most λ values in two datasets.